Technical University of Denmark

Near-field characterization of low-loss photonic crystal waveguides

Volkov, V. S.; Bozhevolnyi, S. I.; Borel, Peter Ingo; Frandsen, Lars Hagedorn; Kristensen, Martin

DTU Library
Technical Information Center of Denmark

Near-field characterization of low-loss photonic crystal waveguides

V. S. Volkov* and S. I. Bozhevolnyi

Department of Physics and Nanotechnology, Aalborg University, Pontoppidanstræde 103, DK-9220 Aalborg Øst, Denmark

P. I. Borel, L. H. Frandsen, and M. Kristensen

Research Center COM, Technical University of Denmark, Oersteds Plads 345V DK-2800 Kgs. Lyngby, Denmark

A scanning near-field optical microscope is used to directly map the propagation of light in the wavelength range of 1500–1630 nm along straight photonic crystal waveguides (PCWs) fabricated on silicon-on-insulator wafers. The PCWs were formed by removing a single row of holes in the triangular 428-nm-period lattices with different filling factors (0.76 and 0.82) and connected to access ridge waveguides. Using the near-field optical images we investigate the light propagation along PCWs for TM and TE polarizations (the electric field is perpendicular/parallel to the sample surface). Efficient guiding (for both samples) of the TM-polarized radiation is observed in the whole range of laser tunability. For TE polarization, the efficient guiding is limited to the wavelengths shorter than 1552 or 1570 nm for the PCW with the filling factor of 0.76 or 0.82, respectively. For longer wavelengths, we observe drastic and rapid deterioration of the waveguiding and PCW mode confinement, ending up with the complete disappearance of the PCW mode once the wavelength exceeds the cutoff value by merely 2 nm. Using averaged cross sections of the intensity distributions along the PCW axis, the propagation loss is evaluated and found to be in good agreement with the corresponding transmission spectra. Considering spatial frequency spectra of the intensity variations along the PCW axis, we determine (for both polarizations) the dispersion of the PCW mode propagation constant and, thereby, the mode group and phase velocities.

PACS number(s): 42.55.Tv, 07.79.Fc, 42.70.Qs, 42.25.−p

I. INTRODUCTION

The development of the integrated optical components based on planar photonic band gap (PBG) structures, also called photonic crystals (PCs), has attracted a great deal of attention.[1] The most interesting applications are related to the possibilities of controlling of photons in PCs by introducing artificial defects and by locally disturbing the PBG. In the last few years, main efforts have been concentrated within systematic theoretical studies[2–4] and experimental investigations[5–9] of different configurations of waveguides and cavities in PC slabs. Differences in guiding mechanisms between conventional dielectric waveguides and line defects in PCs lead one to expect many unique characteristics and properties of PC waveguides (PCWs). For example, it has been predicted that photons can be trapped for long periods of time in point-defect cavities or that wavelength-scale sharp bend with PCWs.[10] Another noticeable feature of PCWs is their dispersion characteristics that are also different from those of conventional waveguides. The experimental methods applied until recently for the characterization of the dispersion and propagation loss in PCWs are often based on the decoding of Fabry–Pérot oscillations in transmission spectra. Several groups have extracted the group velocity dispersion from the phase of Fabry–Pérot oscillations, and extremely large dispersion was observed implying that the mode group velocity was reduced down to 1/100 of the speed of light in air.[11,12] The results of direct observations of the optical properties of two-dimensional (2D) PCWs by using ultrabroadband femtosecond-pulse time-of-flight measurements were also reported.[13] Concerning the dispersion, the surface coupling technique has been applied for direct measurements of the photonic dispersion curves in PCWs.[14,15] Small group velocity (suppressed by two orders of magnitude relative to those in bulk semiconductors) were observed in one-dimensional (1D) patterned AlGaAs waveguides.[15]

Quite recently, we have employed a collection scanning near-field optical microscope (SNOM) for imaging of the propagation of light at telecommunication wavelengths along straight and bent regions of silicon-on-insulator PCWs.[16,17] High-quality SNOM images were obtained allowing us to directly evaluate the bend loss and characterize the PCW mode confinement. Furthermore, by considering spatial frequencies in light-intensity variations along the PCW we have estimated the propagation constant and determined the dispersion of the PCW mode. In this work, we conduct further SNOM investigations of light propagation in straight PCWs that were fabricated on silicon-on-insulator (SOI) wafers with two different filling factors exhibiting distinctly different transmission of TE polarization (electric field parallel to the sample surface plane). Analyzing the SNOM images obtained in the whole wavelength range (1500–1630 nm) of tunability of our laser system, we determine the wavelength range of PCW guiding for both TE and TM polarizations and *directly* evaluate the corresponding propagation losses using averaged cross sections of the SNOM images along the PCW axis. By use of qualitative description of image formation in the collection SNOM and comparing the mode propagation constants with the previously obtained results[16,17] we account for spatial frequency spectra of the intensity variations and determine the dispersion of the PCW mode propagation constant (for both polarizations) used for the evaluation of the corresponding group velocity.
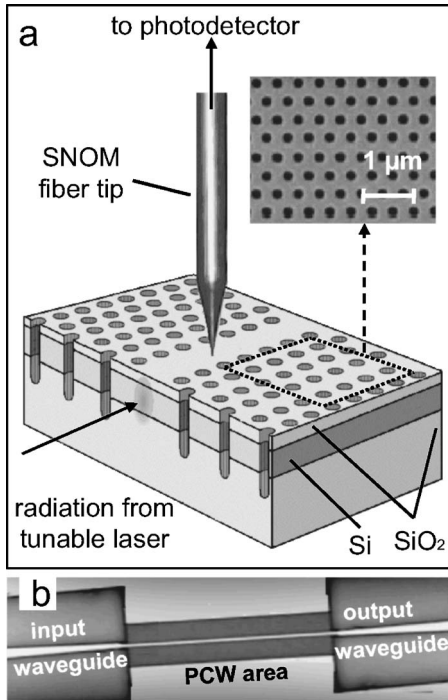
FIG. 1. (a) Schematic layout of the experimental setup. (b) Optical microscope image showing a top view of the central part of the sample, which contains straight PCWs.

II. EXPERIMENTAL ARRANGEMENT

The schematic of the experimental setup is shown in Fig. 1. It consists of a collection SNOM (Ref. 18) with an uncoated fiber tip used as a probe and an arrangement for launching tunable (1500–1630 nm) TM/TE-polarized (the electric field is perpendicular/parallel to the sample surface plane) radiation into the input ridge waveguide by positioning a tapered-lensed polarization-maintaining single-mode fiber. The adjustment of the in-coupling fiber with respect to the sample facet was accomplished when monitoring the light propagation along the sample surface with help of a far-field microscopic arrangement.[5] Following the fiber adjustment, the intensity distribution near the sample surface is probed with an uncoated sharp fiber tip of the SNOM [Fig. 1(a)]. The tip can be scanned along the sample surface at a constant distance of a few nanometers maintained by shear force feedback. Near-field radiation scattered by the tip is partially collected by the fiber itself and propagates in the form of the fiber modes towards the other end of the fiber, where it is detected by a femtowatt InGaAs photoreceiver.

Both samples were fabricated on SOI wafers, consisting of a $SiO_2/Si/SiO_2$ trilayer film (cladding/core/buffer thickness $\sim 0.1/0.3/1$ μm) formed on Si substrate.[19] Sample N1 contained a PC area, in which holes were arranged in a triangular array (lattice constant $\Lambda \cong 428$ nm, hole diameter $\cong 0.76\Lambda$) and single rows of missing holes defined the PCWs along ΓM direction of the irreducible Brillouin zone of the lattice. The sample contained a central PC area (with PCW regions of different lengths) connected to tapered access ridge waveguides outside the PC area as it is shown in Fig. 1(b). Ridge waveguides, gradually tapered from a width of
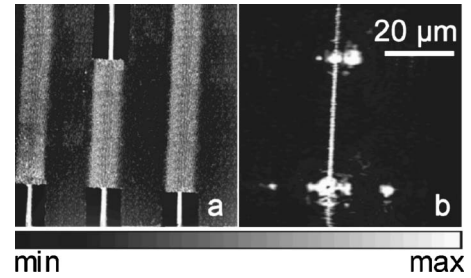

FIG. 2. Grey-scale (a) topographical and (b) near-field optical images (66×66 μm^2) obtained with a 40-μm-long PCW of sample N1 at the wavelength $\lambda \cong 1520$ nm for TM polarization.

~ 4 μm at the sample facet to ~ 1 μm at the PC interface, are used to route the light to and from the PCWs. Sample N2 was similar to N1 but the PCWs were formed in a hole array with $\Lambda \cong 428$ nm and holes diameter $\cong 0.82\Lambda$. Electron (e)-beam lithography was employed for both samples to produce the hole pattern in a resist layer deposited on a (SOI) wafer. The patterned resist served as a mask in the process of reactive ion etching (RIE) resulting in the corresponding pattern of holes formed in the Si layer. After removal of the resist, the pattern was further transferred onto the SiO_2 layer by RIE, using the patterned Si layer as a mask. Finally, samples were thermally oxidized in order to grow a thin SiO_2 layer on top of the Si layer and on the inner walls of the air holes (the silica top cladding increases the vertical symmetry of the structures and smoothens out surface roughnesses of the structures).[19]

III. EXPERIMENTAL RESULTS

For both samples, 40-μm-long PCW were excited at different wavelengths ranging from 1500 to 1630 nm and two different (TE/TM) polarizations and imaged with the SNOM. It should be noted that the SNOM images presented here (Figs. 2–6) are oriented in a way that the light propagates upwards in the vertical direction.

A. Near-field images

Typical topographical and near-field optical images obtained for the PCW (sample N1) at the wavelength of 1520

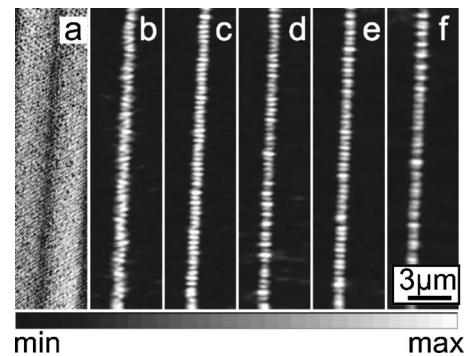FIG. 3. Grey-scale (a) topographical and (b)–(f) near-field optical images (5×25 μm^2) obtained with a 40-μm-long PCW (sample N1) at the wavelengths $\lambda \cong$ (b) 1500, (c) 1520, (d) 1550, (e) 1590, and (f) 1630 nm for TM polarization.

FIG. 4. Grey-scale (a) topographical and (b)–(f) near-field optical images (5×25 μm^2) obtained with a 40-μm-long PCW (sample N1) at the wavelength $\lambda \cong$ (b) 1500, (c) 1522, (d) 1524, (e) 1560, and (f) 1600 nm for TE polarization.

nm (TM polarization) are shown in Fig. 2. On the topographical image [see Fig. 2(a)], the input and output ridge waveguides are clearly seen. One can also easily recognize the PBG structure on the topographical image, but the pattern of holes that forms the PCW following by input and output waveguides is not discernible, because the scanning parameters were not optimized with respect to the topographical imaging. The near-field optical image [Fig. 2(b)] exhibits several features appearing also on the images at other wavelengths. The light propagating along the input ridge waveguide and further in the PCW and along the output waveguide is clearly seen, as well as the light scattering at the junctions between the PCW and ridge waveguides. The light scattering at junctions results in scattered field components propagating (in air) away from the sample surface. These propagating components are detected with the SNOM fiber tip much more efficiently than the evanescent field components,[20] e.g., associated with the PCW and ridge waveguides modes, resulting in the image contrast distortion.[16,17] It should also be noted that the signal does not go to zero outside the PCW indicating the presence of homogeneous background at the level of ~10% compared to the maximum signal.

The features in light propagation along the same straight PCW are more visible in the high-resolution optical images

FIG. 5. Grey-scale (a) topographical and (b)–(f) near-field optical images (5×25 μm^2) obtained with a 40-μm-long PCW (sample N2) at the wavelength $\lambda \cong$ (b) 1500, (c) 1530, (d) 1570, (e) 1600, and (f) 1630 nm for TM polarization.
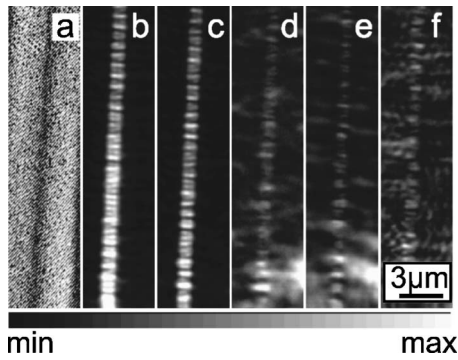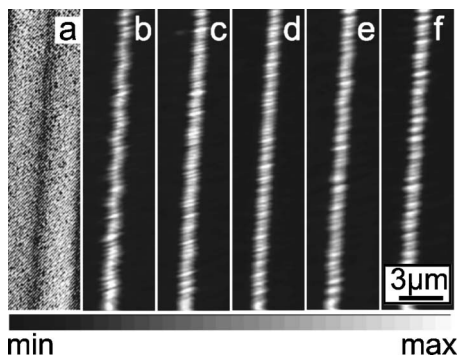

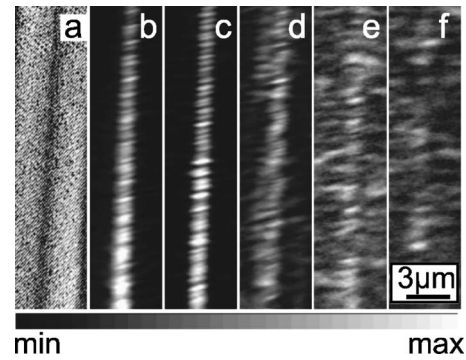FIG. 6. Grey-scale (a) topographical and (b)–(f) near-field optical images (5×25 μm^2) obtained with a 40-μm-long PCW (sample N2) at the wavelength $\lambda \cong$ (b) 1500, (c) 1570, (d) 1572, (e) 1590, and (f) 1630 nm for TE polarization.

exhibiting spatial periods down to 300 nm (Figs. 3 and 4). It is seen that the recorded intensity distributions are well confined (to the line of missing holes defining the PCW) exhibiting wavelength-dependent intensity variations along the propagation direction. For TM polarization, the efficient guiding along the PCW was observed in the whole wavelength range (1500–1630 nm) of tunability of our laser system (Fig. 3). The interference fringes along the PCW are well pronounced and indicating the reflection from the waveguide termination. The signal cross sections (not shown here) made at intensity maxima are close to the Gaussian distributions in shape with the full width at half maximum (FWHM) increasing from ~760 to 788 nm with the increase of the light wavelength. For TE polarization, the efficient guiding was observed in the wavelength range of 1500–1522 nm [Figs. 4(b) and 4(c)]. We found drastic changes in the PCW guiding and mode confinement with further increase of the light wavelength by merely 2 nm [Fig. 4(d)]. No PCW mode was observed at longer wavelengths [Figs. 4(e) and 4(f)]. Such a critical wavelength dependence of the PCW mode characteristics is, in our opinion, a direct consequence of the well-defined PBG effect in the structure.

The SNOM images obtained for the PCW having the filling factor of ~0.84 (sample N2) in the whole laser tunability range exhibit the efficient guiding along PCW in the wavelength range of 1500–1630 nm for TM polarization and 1500–1570 nm for TE polarization (Figs. 5 and 6, respectively). Within these ranges, the optical image cross sections (averaged over a few lines) made at intensity maxima demonstrate well-confined mode intensity distributions with the FWHM being ~1.1 and 1.75 μm, correspondingly for TM and TE polarizations. Similarly to the guiding of TE polarization in the PCW of sample N1, the TE mode disappeared rapidly once the light wavelength increased by 2 nm over the PBG edge (from 1570 to 1572 nm). The comparison of the results obtained indicates clearly and unambiguously that the long-wavelength edge of the PBG shifts towards the longer wavelengths with the increase of the filling factor.

B. Determination of the propagation loss

Using the SNOM images obtained at different wavelengths (Figs. 3–6), we have directly determined the propa-
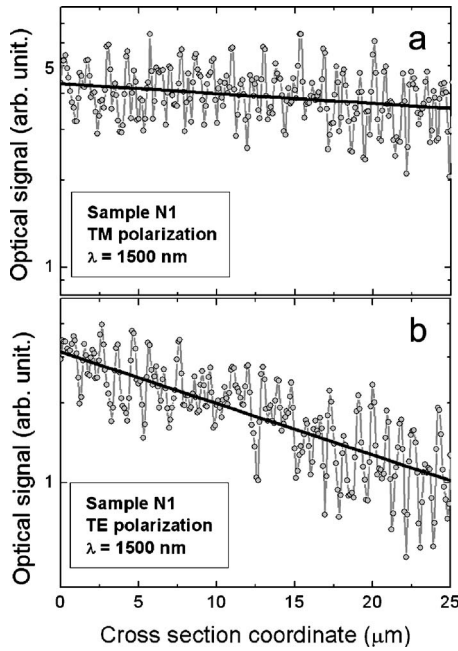
FIG. 7. Averaged cross sections of the near-field optical images shown in Figs. 3(b) and 4(b) along the PCW axis. Solid lines indicate linear fits to the experimental data.

gation loss by averaging over 11 profiles of the intensity distributions that were cut along the ($\sim$25-μm-long) PCW axis. Variations in the detected signal along the PCW axis made the precise evaluation of the propagation loss rather difficult. For different wavelengths, the propagation losses were extracted by finding the slopes of the best linear fits to the corresponding average cross sections (Fig. 7). The obtained results (recalculated as transmission through the 10 -μm-long PCW of sample N1 and the 40-μm-long PCW of sample N2) are shown in Fig. 8 along with the transmission measurements conducted with the same samples (using the conventional approach of measuring the transmission spectra for PCWs of different lengths.[19]) This experimental technique is widely used for the characterization of PCW structures and based on usage of optical fibers for coupling the
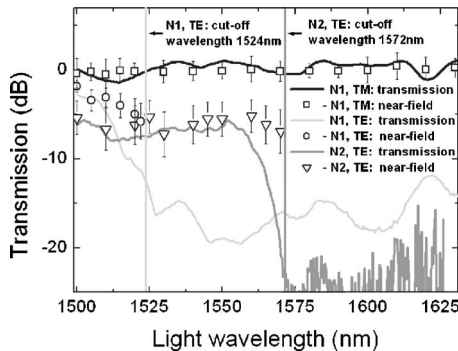

FIG. 8. Transmission spectra measured with a 10-μm-long PCW of sample N1 (black line corresponds to TM polarization, light gray line—to TE polarization) and 40-μm-long PCW of sample N2 (gray line) plotted together with the results obtained from the averaged cross sections of SNOM images.

light in and out of the PCWs. In this case, the light source was a broadband light emitting diode (LED) and the optical spectra for the transmitted light were recorded with a spectral resolution of 10 nm using an optical spectrum analyzer.[21] A direct comparison between the experimental transmission spectra and the data obtained from the corresponding SNOM images (Fig. 8) shows rather good correspondence in the wavelength ranges of mode guiding as seen from the SNOM images (Figs. 4 and 6). At the same time, this comparison indicates that the conventional technique of characterization is somewhat misleading as it does not provide a clear evidence of the PCW mode cutoff behavior, showing instead a gradual decrease in the transmission. It is also seen that the transmission measurements tend to overestimate the propagation loss near the PBG edge probably because the coupling between access ridge waveguides and PCWs becomes unstable (due to a drastic increase in the FWHM of PCW modes). This means in turn that large propagation losses usually reported for the PCW modes close to the PBG edges (that are interesting due to high dispersion and low group velocities) might be a result of overestimation. It should be borne in mind that the difference in spectral resolution of measurements performed using the tunable laser and LED might also have influenced the transmission curves obtained (e.g., by smoothening the transmission curve measured with the LED).

C. Dispersion of the mode propagation constant

The SNOM images obtained with high resolution at different light wavelengths for a straight region of the PCWs (for samples N1 and N2) are shown in Figs. 3–6. The periodic intensity patterns seen along the propagation direction can be related to the interference between fiber modes excited by the SNOM fiber tip interacting with both evanescent fields and weak optical fields forming a quasihomogeneous background.[16] All these plane wave components contribute linearly to the amplitude of the fiber modes propagating toward a photodetector. Therefore, in the SNOM imaging of the waveguide modes, especially those with large effective indexes, even weak scattered optical fields caused by material inhomogeneities and fabrication defects can contribute to the detected signal. This contribution being coherent and most strong from the optical fields with small wave vector projections results in an interference pattern superimposed on the image formed by a waveguide mode. Such an interference pattern is somewhat irregular due to different contributing plane wave components, exhibiting the interference fringes corresponding to the optical field with zero wave vector projection (propagating away from the surface) i.e., to the homogeneous coherent background.

In the case of the PCW oriented along the x axis, the field probed by the SNOM above the sample surface and along the PCW can be approximated as follows:[5,16]

$$E_d(x,z) = B + \sum_m u_m^0$$

$$\times \exp\left[-z\sqrt{(\beta+mK)^2 - k_0^2}\right]\exp[i(\beta+mK)x],$$

$$\tag{1}$$

where $K = 2\pi/\Lambda, m = 0, \pm 1, \pm 2, \ldots$, the z axis is perpendicu-
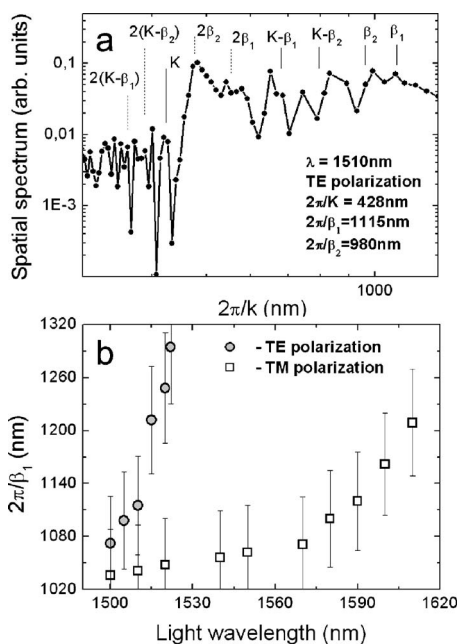
FIG. 9. (a) Spatial frequency spectrum of the optical image obtained with the PCW of sample N1 for TE polarization at the wavelength $\lambda \cong 1510$ nm. Positions of the main peaks fitted to the experimental data are indicated with solid lines. Dotted lines indicate combination frequencies that may appear due to the propagating backward PCW modes and/or nonlinear detection. (b) Wavelength dependence of the propagation constant of the main PCW mode determined from the corresponding near-field optical images obtained for TM and TE polarizations.

lar to the sample surface ($z=0$) pointing to the air side, B represents a homogeneous background, $k_0=2\pi/\lambda$ is the wave number in air, u_m^0 is the amplitude of the main electric field component of the PCW mode having the propagation constant β, Λ is the PC lattice constant, and it is assumed that all Bloch components are evanescent. Each of the field components described in Eq. (1) contribute to the fiber mode amplitude (which is actually detected), though the coupling efficiency decreases with the increase of the wave vector surface projection $|\beta+mK|$.[16,20] One reason is that the effective detecting center of a SNOM probe fiber is situated at some distance inside the fiber (up to 500 nm), so that the evanescent fields are always probed at a nonzero distance from the surface.[22] This consideration can be generalized for the case of two PCW modes having the propagation constants β_1 and β_2.[17] In this case, the dominating signal harmonics would be those with spatial frequencies $\beta_1, \beta_2, K-\beta_1$, and $K-\beta_2$. The occurrence of several PCW modes might be caused by excitation of different depth modes of the input ridge waveguide. One can also expect that some of the PCW modes would be actually index-guided modes.

We investigate in detail the light propagation in the PCW of sample N1 for both polarizations. The typical spatial frequency spectrum of the optical signal variations along the PCW is shown (for TE polarization) in Fig. 9(a) for the light wavelength of 1510 nm. The spectrum features several peaks that can be assigned, in agreement with the arguments given above, to the spatial frequencies of two PCW modes with the

propagation constants β_1 and β_2. The lattice constant 428 nm of this PC was obtained from images made by a calibrated scanning electron microscope. The PCW mode propagation constants β_1 and β_2 were fitted to the experimental spectrum so that the frequencies $K-\beta_1$ and $K-\beta_2$ would also fit to the corresponding peaks as shown in Fig. 9(a). It is seen that the spectrum structure, being well defined at low spatial frequencies, is more complicated at high spatial frequencies. Such a structure might be related to the reflected PCW modes by the PCW-ridge waveguide interface and/or the output edge of the sample. Comparing current observations with the results of our previous work[16,17] we conjecture that the mode with β_1 is the main (true) PCW mode. The mode with β_2 is the most probably only index guided and excited due the multi-mode light propagation in the input ridge waveguide. The above fitting procedure was carried out for other wavelengths (for both polarizations) resulting in the wavelength dependence of the PCW mode propagation constant β_1 [Fig. 9(b)]. We can further identify the following reasons of uncertainty in the determination of mode propagation constants: the fact that the background contribution consists of many propagating field components with small but not zero wave vector projections on the surface plane, and a finite length of the corresponding cross sections (~ 25 μm in this case). Nevertheless, the results obtained indicate that the propagation constant of the PCW mode varies faster than that of free propagating light in air, for example (for TE polarization), when the ratio Λ/λ varies from 0.28 to 0.29 the ratio Λ/λ_{PCW} changes from 0.33 to 0.41 [see Fig. 9(b)]. Such dispersion is actually expected for the PCW mode in silicon-on-insulator PBG structures.[23] Considering the wavelength dependence of the propagation constant determined from the corresponding spatial spectrums, we calculated the phase and group velocities for TM-polarized and TE-polarized PCW modes in the wavelength range of 1500–1610 nm. The results obtained were normalized with respect to the speed of light in vacuum and plotted in Fig. 10. It is clearly seen that the group velocity rapidly decreases, reaching the values of $\sim 0.11c$ at $\lambda \cong 1610$ nm for TM polarization and $\sim 0.035c$ at $\lambda \cong 1522$ nm for TE polarization, as the wavelength increases towards the PBG edge [Figs. 10(a) and 10(b), respectively]. At the same time, the phase velocity does increase though relatively slow so that the PCW mode constant becomes closer to the light line in air for longer wavelengths. It should be mentioned that this behavior of the group velocity is in agreement with the results reported recently.[24] In the referred experiment, the group velocity being equal to one-twentieth the speed of light in vacuum was observed at a frequency near the edge of the waveguide mode for time-domain measurements of picosecond light-pulse propagation in a 2D PCW.

In order to understand the underlying physics of what we observed, the theoretical TE/TM band structure diagrams were calculated for the PCW by directly solving time-dependent Maxwell equations with the three-dimensional (3D) finite-difference time-domain (FDTD) method.[25] The calculated dispersion curves are rather complicated (Fig. 11), but they are basically reflecting two main guiding mechanisms: the PBG guiding (for TE polarization) [Fig. 11(a)] that leads near the PBG edge to significant changes in the
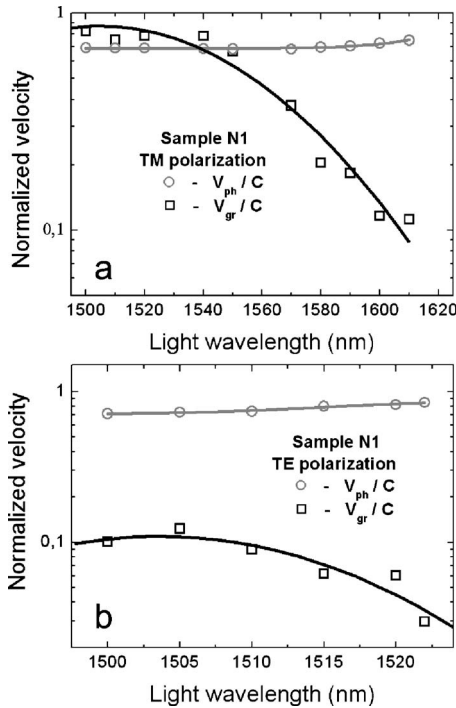
FIG. 10. Group and phase velocities normalized to the speed of light in vacuum for the (a) TM-polarized and (b) the TE-polarized PCW mode of sample N1 as functions of the light wavelength. Solid lines (used to guide the eye) represent quadratic approximations by the least-square method.

FIG. 11. 3D FTDT calculated (a) TE and (b) TM band diagrams with the light line indicated. Black lines represent (a) the PBG guided mode and (b) the refractive-index guided mode. Note that the group velocity being proportional to the slope of a dispersion curve is expected to become very small at the edge of the Brillouin zone.

propagation constant with the light wavelength [Figs. 9(b) and 11(a)] and the refractive-index guiding (for TM polarization) [Fig. 11(b)]. From the TM-band diagram, it is clearly seen that there is no PBG for TM polarization, a circumstance that reveals pure effective-refractive-index guiding of TM mode (similar to the conventional dielectric waveguiding). This feature accounts for broadband transmission of TM polarization that affected weakly (if at all) by the PBG structure. Note also that the calculated TM (TE) dispersion curve occupies a very large (small) frequency interval below the light line that is also in agreement with the results obtained from SNOM images [e.g., Fig. 9(b)].

IV. CONCLUSIONS

Using the collection SNOM, we have imaged the propagation of light at telecommunication wavelengths along straight PCWs (with different filling factors), which were formed by removing a single row of holes in the triangular 428-nm-period lattice. High quality SNOM images of these waveguides excited in the wavelength range 1500–1630 nm have been obtained and used to characterize the PBG structures studied. Using the near-field optical images we have directly investigated the light propagation along PCWs for TE and TM polarizations. The efficient guiding (for both samples) of the TM-polarized radiation was observed in the whole range of laser tunability. At the same time, for TE polarization, the efficient guiding was limited to the wavelengths shorter than 1552 or 1570 nm for the PCW with the
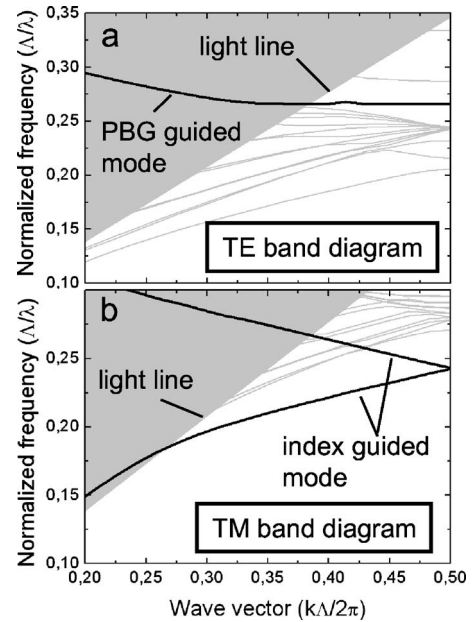
filling factor of 0.76 or 0.82, respectively. For longer wavelengths, we have observed drastic and rapid deterioration of the waveguiding and PCW mode confinement, ending up with the complete disappearance of the PCW mode once the wavelength exceeded the cutoff value by merely 2 nm. Such a critical wavelength dependence of the PCW guiding (for TE polarization) is, in our opinion, a clear evidence of the well-defined PBG effect in the structure. We have also found that long-wavelength PBG edge shifted towards longer wavelengths with the increase of the filling factor, emphasizing thereby the fact that the filling factor is an important design parameter for PCWs. Using averaged cross sections of the intensity distributions along the PCW axis, the propagation loss has been evaluated and found to be in good agreement with the corresponding transmission spectra. We have also discussed several delicate issues that should be borne in mind when conducting the PCW characterization using the conventional approach of measuring the transmission spectra. Finally, considering spatial frequency spectra of the intensity variations along the PCW axis, we determine (for both polarizations) the dispersion of the PCW mode propagation constant and, thereby, the mode group and phase velocities. Our results indicate that the group velocity decreases rapidly when the wavelength approaches the long-wavelength PBG edge, reaching the values of $\sim 0.11c$ (for TM polarization) and $\sim 0.035c$ (for TE polarization) as the wavelength approaches to ~ 1610 and 1522 nm, correspondingly. The experimentally established large dispersion and significant reduction in the group velocity (directly related to the tight confinement and strong Bragg scattering in the PCW) were also corroborated with the theoretical dispersion curves calculated with the 3D FDTD method.

The results presented in this work have not only corroborated the already reported findings, e.g., regarding the decrease in the PCW mode group velocity near the PBG edge,[24,26] but also demonstrated the alternative method of determination of the PCW group velocity, which is a very important characteristic of the PCW mode (also from point of view of potential applications in optical delay lines). We believe that the reported results can help in designing further, more detailed and accurate, SNOM investigations of PCWs as well as in avoiding pitfalls when applying the conventional characterization techniques. The accurate PCW characterization is particularly important since rigorous calculations of the properties of PCW components are extremely difficult and time consuming. Finally, we believe that the SNOM imaging can be used not only to quantitatively characterize properties of fabricated PCWs and PC structures (mode content, dispersion, insertion loss, and identification of loss channels) and thereby optimize their performance, but also to elucidate physical mechanisms in various intriguing scattering phenomena occurring in PCs.

---

*Author to whom correspondence should be addressed; Email address: volkov@physics.auc.dk

[1] J. D. Joannopoulos, P. R. Villeneuve, and S. Fan, Nature (London) **386**, 143 (1997).

[2] S. G. Jonson, P. R. Villeneuve, S. Fan, and J. D. Joannopoulos, Phys. Rev. B **62**, 8212 (2000).

[3] A. Chutinan and S. Noda, Phys. Rev. B **62**, 4488 (2000).

[4] O. Painter, J. Vuckovic, and A. Scherer, J. Opt. Soc. Am. B **16**, 275 (1999).

[5] M. Lončar, D. Nedeljkovic, T. P. Pearsall, J. Vuckovic, A. Scherer, S. Kushinsky, and D. C. Allan, Appl. Phys. Lett. **80**, 1689 (2002).

[6] T. F. Krauss and R. M. De La Rue, Prog. Quantum Electron. **23**, 51 (1999).

[7] P. I. Borel, L. H. Frandsen, M. Thorhauge, A. Harpøth, Y. X. Zhuang, and M. Kristensen, Opt. Express **11**, 1757 (2003).

[8] O. Painter, R. K. Lee, A. Yariv, A. Scherer, J. D. O'Brien, I. Kim, and P. D. Dapkus, Lasers and Electro-Optics CPD21/1 (1999).

[9] S. Y. Lin, E. Chow, S. G. Jonson, and J. D. Joannopoulos, Opt. Lett. **26**, 1903 (2001).

[10] A. Mekis, J. C. Chen, I. Kurland, S. Fan, P. R. Villeneuve, and J. D. Joannopoulos, Phys. Rev. Lett. **77**, 3787 (1996).

[11] X. Letartre, C. Seassal, C. Grillet, P. Rojo-Romeo, P. Viktorovich, M. Le Vassor d'Yerville, D. Cassagne, and C. Jouanin, Appl. Phys. Lett. **79**, 2312 (2001).

[12] M. Notomi, K. Yamada, A. Shinya, J. Takahashi, C. Takahashi, and I. Yokohama, Phys. Rev. Lett. **87**, 253902 (2001).

[13] M. C. Netti, C. E. Finlayson, J. J. Baumberg, M. D. B. Charlton, M. E. Zoorob, J. S. Wikinson, and G. J. Parker, Appl. Phys. Lett. **81**, 3927 (2002).

[14] V. N. Astratov, I. S. Culshaw, R. M. Stevenson, D. M. Whittaker, M. S. Skolnick, T. F. Krauss, and R. M. De La Rue, J. Lightwave Technol. **17**, 2050 (1999).

[15] V. N. Astratov, R. M. Stevenson, I. S. Culshaw, D. M. Whittaker, M. S. Skolnick, T. F. Krauss, and R. M. De La Rue, Appl. Phys. Lett. **77**, 178 (2000).

[16] S. I. Bozhevolnyi, V. S. Volkov, T. Søndergaard, A. Boltasseva, P. I. Borel, and M. Kristensen, Phys. Rev. B **66**, 235204 (2002).

[17] S. I. Bozhevolnyi and V. S. Volkov, Philos. Trans. R. Soc. London, Ser. A **362**, 757 (2004).

[18] DME-DualScope™, Herlev, Denmark.

[19] J. Arentoft, T. Søndergaard, M. Kristensen, A. Boltasseva, M. Thorhauge, and L. Frandsen, Electron. Lett. **38**, 274 (2002).

[20] S. I. Bozhevolnyi, B. Vohnsen, and E. A. Bozhevolnaya, Opt. Commun. **172**, 171 (1999).

[21] P. I. Borel, L. H. Frandsen, M. Thorhauge, A. Harpøth, Y. X. Zhuang, and M. Kristensen, Opt. Express **11**, 1757 (2003)

[22] A. Nesci, R. Dändliker, M. Salt, and H.-P. Herzig, Opt. Commun. **205**, 229 (2002).

[23] T. Søndergaard, J. Arentoft, and M. Kristensen, J. Lightwave Technol. **20**, 1619 (2002).

[24] T. Asano, K. Kiyota, D. Kumamoto, B.-S. Song, and S. Noda, Appl. Phys. Lett. **84**, 4690 (2004).

[25] A. Lavrinenko, P. I. Borel, L. H. Frandsen, M Thorhauge, A. Harpøth, M. Kristensen, and H. M. H. Chong, Opt. Express **11**, 1757 (2003).

[26] H. Gersen, T. J. Karle, R. J. P. Engelen, W. Bogaerts, J. P. Korterik, N. F. Van Hulst, T. F. Krauss, and L. Kuipers, Phys. Rev. Lett. **94**, 073903 (2005).